Nanoscale Advances

Accepted Manuscript

Chiral induction in the crystallization of KIO₃ and LiIO₃, the role of amino acids in controlling the chirality of inorganic crystals.

Matan Oliel,*[a] and Yitzhak Mastai [b]

Department of Chemistry and Institute of Nanotechnology, Bar-Ilan University, Ramat-Gan 5290002, Israel

Chiral induction in crystals attract significant attention due to its implications for developing chiral materials and understanding mechanisms of symmetry- breaking enantioselective crystallization of naturally occurring chiral minerals. Despite its potential use in chiral discrimination, this area remains largely unexplored. Here, we investigate chiral induction during crystallization of naturally occurring chiral KIO_3 and $LiIO_3$ minerals using arginine and alanine as chiral inducers. The chiral nature of the crystallization and the effect of the chiral inducers were examined using circular dichroism, polarimetry, and low-frequency Raman spectroscopy. The impact of chiral molecules on the rate and final crystal structure was studied by electron microscopy including SEM and TEM. We demonstrate that it is possible to control the chirality with chiral exogenous molecules, mainly amino acids. Understanding chiral induction in crystal growth may open avenues for controlled assembly of chiral materials and development of novel functional materials with unique properties.

Introduction

Chirality is often associated with organic molecules; however, many inorganic compounds also exhibit chirality in their crystal structures. This chirality in inorganic crystals generally results from a chiral arrangement of non-centrosymmetric metal chelates or oxides. For instance, quartz (SiO_2) demonstrates chirality in its α polymorph due to the chiral arrangement of SiO_2 units.

Studying the chirality of chiral inorganic crystals is surprisingly limited[1]. The surface of chiral inorganic crystals holds significant promise for various applications including chiral discrimination[2-5], chiral sensing[6] and enantioselective catalysis[7,8]. Understanding how surface chirality is influenced by chiral induction and controlling chirality in these materials is crucial, as chiral selectivity occurs primarily on the material surface[9].

In recent years, chirality has been found to play an important role in nanotechnology[10-12]. Chirality plays a useful role in many nano-systems, such as chiroptical molecular switches[13-15], molecular motors, chiral nanosurfaces[16-26] and chiral nanoparticles[27-39]. Overall, the areas of chiral nanoscience and nanotechnology show exceptionally strong promise for further developments in areas such as catalysts, bio-recognition and chiral separation processes[40].

One good example of chiral surfaces is chiral selectivity on metal surfaces that are well-established, in particular with cubic closed-packed (CCP) metals[41]. Crystal planes such as Cu

(6,4,3) and Au (3,2,1) exhibit chiral properties despite the lack of chirality of bulk metals. These surface features yield exceptional enantiomeric excess (e.e) during adsorption of small chiral molecules[4,42].

In recent decades, remarkable strides were taken in exploring the nature of inorganic chiral surfaces and systems. Pioneering research led by the Gellman group unveiled the chirality of high-Miller-index planes in metallic surfaces, revealing their enantiospecific adsorption in the presence of chiral molecular probes[6,17]. Research led by Hazen and collaborators emphasized the significance of chiral inorganic crystal surfaces, in particular in mineral-catalyzed organic synthesis and the interactions between biomolecules and mineral surfaces[1,43,44]. In a series of publications, Hazen *et al.* carefully documented numerous common rock-forming minerals, predominantly chiral oxides and silicates, which exhibit chiral crystal surfaces, showcasing the chiral selection of amino acids on these surfaces[45,46].

However, naturally occurring chiral minerals including quartz (SiO_2)[47], Monohydrocalcite $(CaCO_3 \cdot H_2O)$[48], Wulfingite (ε-$Zn(OH)_2$)[49] and α-HgS[50,51] received little attention. Some chiral minerals are believed to contribute to the development of homochirality in biological molecules through an extensive process of chiral discrimination[52,53]. Studying the influence of chiral amino acids on formation of chiral minerals and replicating the natural conditions in which this occurs provides valuable insights into these processes. This research can also elucidate mechanisms that control chiral biomolecules. While some chiral minerals form the chiral phase in a straightforward manner, the crystallization of certain chiral crystals is more complex. For example, Berlinite, the quartz-like chiral form of $AlPO_4$, requires high annealing temperatures to transform into its chiral phase[54,55]. These extreme conditions present challenges for analysis of chiral induction.

To address this issue, we sought chiral inorganic systems that crystallize under relatively simple conditions, mainly at low temperature and in aqueous solutions. Potassium iodate (KIO_3)[56,57] and lithium iodate $(LiIO_3)$[58,59] are perfect examples. KIO_3 and $LiIO_3$ are naturally occurring chiral minerals with space groups of P1 and P6322, respectively, which are easy to crystallize, and their chiral phases are stable at room temperature (RT). As water-soluble salts, their chirality and chiral induction were apparently not investigated.

Here, we present our research on control of chirality of KIO_3 and the $LiIO_3$ crystals by chiral induction with amino acids. The crystal morphology and structural changes were confirmed by X-ray diffraction (XRD), Fourier transform infrared (FTIR) spectroscopy and high-resolution scanning electron microscopy (HR-SEM). Moreover, the chirality was analyzed by circular dichroism (CD) spectroscopy of crystal pellets and optical polarizer for low-frequency Raman (LFR). The enantioselectivity and chiral discrimination was proved by CD and polarimeter by chiral adsorption experiments.

Experimental methods

Materials

The materials used in this research are detailed in the supporting information (S1).

Preparation of chiral-induced crystals

Chiral-induced KIO_3 crystals were synthesized by recrystallization with slow cooling method. Supersaturated solutions in double distilled water (DDW) were prepared, heated to 50 °C and stirred until complete dissolve. After dissolution, 10% (moles / to KIO_3 moles) of L/D-Arg were added and the solution was stirred for 15 min and spontaneusly cooled to RT by turning off the hot plate and keep the solution on it to allow as slow as possibile cooling process and then the solution refrigerated overnight. The white crystals were filtered in vacuum, washed several times with ethanol to remove Arg traces and dried at RT.

The chiral-induced $LiIO_3$ crystals were synthesized by slow evaporation method using the following reaction:

$$Li_2CO_3 + 2HIO_3 \rightarrow 2LiIO_3 + H_2O + CO_2$$
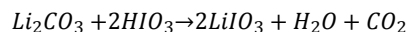
In a typical case 0.5 g of lithium carbonate (Li_2CO_3) and 2.375 g of iodic acid (HIO_3) were dissolved in 20 mL of DDW. The solutions were put in oil bath and heated to 60 °C under stirring at pH = 10 to allow the reaction to occur. The basic conditions were achieved by adding lithium hydroxide (LiOH). After dissolution, 60.6 mg of L/D-Ala (10% mole of Li_2CO_3) were added and the solution was covered by pierced aluminum foil to prevent contamination and allow evaporation. The stirring was stopped after 24 h and the heating was kept at 60 °C in oil bath to maintain constant temperature until complete evaporation. To remove residual Ala, clear white crystals were soaked for 24 hours in 9:1 MeOH/DDW in a glass beaker. The cleaned crystals were filtered and dried in an oven at 50 °C.

Characterization methods

The crystallographic structures of KIO_3 and $LiIO_3$ were determined by XRD using a Bruker AXS D8 Advance diffractometer with Cu Ka (λ = 1.5418 Å) operating at 40 kV/40 mA, collecting from 10 to 80 °.

FTIR was performed using a Thermo Scientific Nicolet iS10 spectrometer equipped with a Smart iTR attenuated total reflectance sampler with a single bounce diamond crystal.

Data was collected in the 530–4000 cm^{-1} range at a spectral resolution of 4 cm^{-1} and analyzed using OMNIC software.

HR-SEM images were taken using a field-emission FEI (Helios 600) instrument. Samples were sputtered with gold.

KIO$_3$ and LiIO$_3$ crystal's chirality measurements

Pellets (KBr, 300 mg, 5/10% L/D-induced Li/KIO$_3$) were prepared (mixed and pressed under 10 ton for 3 min) and measured by CD in a designated holder at different orientations at RT with a Chirascan spectrometer (Applied Photophysics, UK).

LFR was carried out on a Via Raman microscope (Renishaw, UK) at RT under optical microscope with a 50× objective. The samples were excited using a 514 nm laser source with a P-polarization (vertical) ratio of 100:1 (0.5 mW, 40 s) and spectra were acquired using a polarizer with 1800 l/mm grating in the range of 100–1500 cm^{-1}.

Chiral adsorption onto KIO$_3$ and LiIO$_3$ crystals

Tartaric acid (TA) was chosen due its solubility in ethanol in which KIO$_3$ and LiIO$_3$ are insoluble. Chiral adsorption measurements were carried out with CD by preparing a 2.5 mM solution of D/L-TA or DL-TA in ethanol and adding L-Arg-induced KIO$_3$ crystals or L/D-Ala-induced LiIO$_3$ in several concentrations. The crystals were kept suspended in solution overnight using a rotary suspension mixer and filtered out using a 0.2 mm filter. The filtered solutions were taken to CD measurement and compared to pure D/L-TA or DL-TA solutions.

Chiral adsorption by polarimeter was performed by preparing a 5 wt% solution of D/L-TA in ethanol and adding L-Arg-induced KIO$_3$ or L-Ala-induced LiIO$_3$ crystals in several concentrations. The crystals were kept suspended in solution overnight using a rotary suspension mixer and filtered out using a 0.2 mm filter. The filtered solutions were taken to polarimeter measurement and compared to pure D/L-TA solutions. The solutions were measured at RT by a Jasco P-2000 polarimeter.

The selectivity was calculated by measuring the polarization ratio of the enantiomer (adsorption peak maxima) with respect to the pure enantiomer.

For the selectivity measurement by mass change were carried out by preparing a 20 mM of D/L-TA solution in ethanol and adding D-Ala-induced LiIO$_3$ in concentration of 32 mg/mL. The crystals were kept suspended in solution overnight using a rotary suspension mixer and filtered out using a 0.2 mm filter. The filtered solutions were evaporated and the mass change calculated compared to the mass of D/L-TA before the adsorption.

Results and discussion

Characterization

First, we studied the changes in structure and morphology by XRD and FTIR following chiral induction by amino acids. In all samples, the main crystalline structure of KIO$_3$ at RT was the stable triclinic phase with chiral space group P1 (COD ID: 4318187) and main diffraction peak at 2θ = 28.2° corresponding to its (2, -2, 2) plane (Figure 1I). The cell units a, b, c are 8.923, 8.942, 7.709 Å and α, β, γ are 54.4, 125.3, 90.6°. The unchanged diffractions indicate that the crystalline structure is maintained. LiIO$_3$ displays a crystalline structure that fits the RT stable hexagonal phase with chiral space group P6$_3$22 (COD ID: 1529711). The key diffraction peak at 25.5° corresponds to the (1, 0, 1) plane (Figure 1II). The unit cell dimensions were a = 5.478 Å, b = 5.478 Å, c = 5.17 Å with α = β = 90° and γ = 120°. Similar to KIO$_3$, the consistent results indicate that the structure was maintained.

We also characterized the crystals by FTIR to check for structural changes or traces of amino acid. Both pristine and chiral-induced KIO$_3$ showed the same spectra and indicated two peaks, close to each other, with a broad peak at 722 cm^{-1} and a very small peak at 797 cm^{-1}. Both peaks represent the vibration modes of the oxygen-iodine bonds (Figure S2I). Similarly, the LiIO$_3$ crystals showed two peaks belonging to the O-I vibration modes and no difference between the pristine and chiral induced crystals (Figure S2II). However, we noticed a redshift at 763 and 860 cm^{-1} probably due to the effect of the cation on the vibration mode energies in the lattice. Moreover, the control LiIO$_3$ sample also has a broad absorbance peak between 1400, and 1700 cm^{-1} associated with C=O indicating some unreacted Li$_2$CO$_3$.
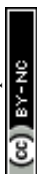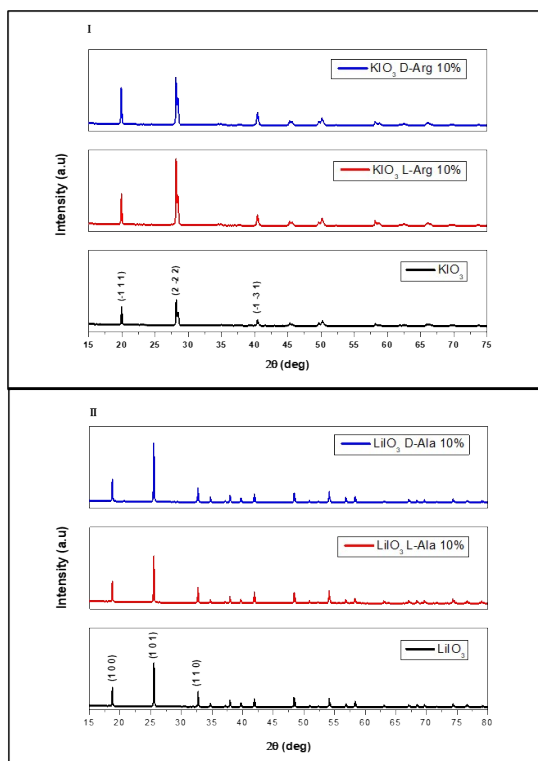
Figure 1 – XRD of KIO$_3$ (I) and LiIO$_3$ crystals (II) – control (black), L-Arg-induced (red) and D-Arg-induced (blue) displaying the main diffraction planes of triclinic KIO$_3$ and hexagonal LiIO$_3$.

Morphology and surface analysis

The morphology was examined by HR-SEM. The control KIO$_3$ crystals exhibit a square shape and smooth surface (Figure 2I, IV) however, with the amino acid the morphology and surface change. The L-Arg-induced KIO$_3$ crystals maintain a square shape albeit with a rough surface (Fig. 2II, V), while the D-Arg-induced KIO$_3$ crystals are hexagonal with a smooth surface similar to the control (III, VI).

Figure 2 – HR-SEM images of KIO$_3$ crystals – control (I, IV / 10, 20 μm), L-Arg-induced KIO$_3$ (II, V / 10, 50 μm) and D-Arg-induced KIO$_3$ (III, VI / 30, 50 μm).

Figure 3 presents HR-SEM images of LiIO$_3$ crystals. Pristine LiIO$_3$ shows an uneven morphology and very rough surface (I, IV). In contrast, L-Ala-induced LiIO$_3$ crystals have a more hexagonal shape with a smoother surface (II, V). D-Ala-induced LiIO$_3$ crystals have an uneven morphology similar to pristine LiIO$_3$ with a rougher surface, which is smoother than the surface of pristine LiIO$_3$ (III, VI).
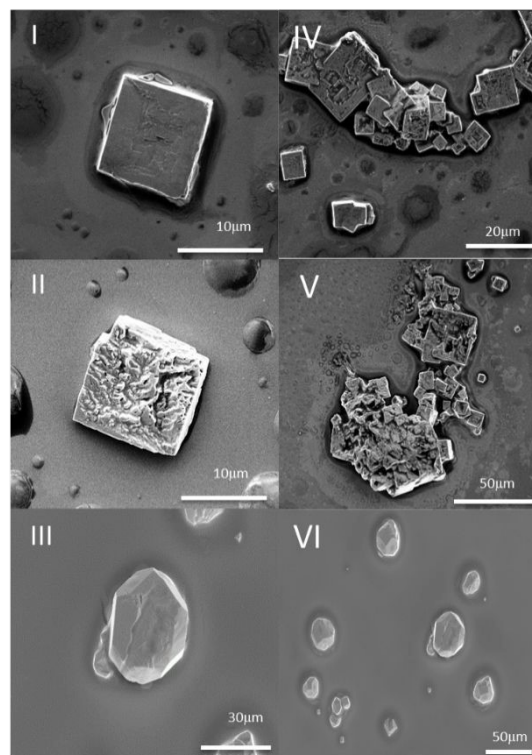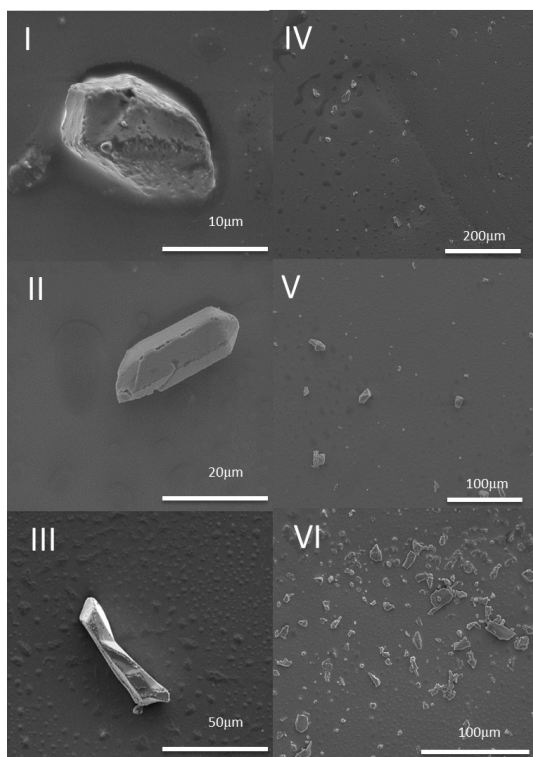
Figure 3 – HR-SEM images of LiIO$_3$ crystals – control (I, IV / 10, 200 μm), L-Ala-induced LiIO$_3$ (II, V / 20, 100 μm) and D-Ala-induced LiIO$_3$ (III, VI / 50, 100 μm).

Direct chirality measurements

To prove the chiral preference, we measured the crystals with CD and LFR. For CD measurement, L/D-Arg-induced KIO$_3$ and L/D-Ala-induced LiIO$_3$ pellets were prepared and measured at different angles. The CD measurement of the chiral-induced KIO$_3$ crystals show two chiral signal areas: a wide one from 525 to 275 nm, and narrow one below 525 nm.

Moreover, a positive signal is seen for the D-Arg-induced crystals and a negative one (anticlockwise direction polarization) for L-Arg-induced KIO$_3$ (Figure 4I). In contrast, LiO$_3$ (Figure 4II) presents opposite signals – positive for L-Ala-induced LiIO$_3$ and negative for D-Ala-induced LiIO$_3$. LiIO$_3$ crystals also display a wide chiral signal from 600 to 400 nm. Both CD spectra show the optical activity of the iodate crystals proving their chiral preference.

While this measure does not provide absolute chirality, the relative purity can be obtained by the most frequent polarizations. The polarization of L-Ala-induced LiIO$_3$ is +4 mdeg *vs.* -6 mdeg for D-Ala-induced LiIO$_3$, thus the latter crystals are 1.5 times purer. L-Arg-induced KIO$_3$ is 1.2 times purer than the D-Arg-induced crystals (-15/+12.5 mdeg for L/D-Arg-induced KIO$_3$).
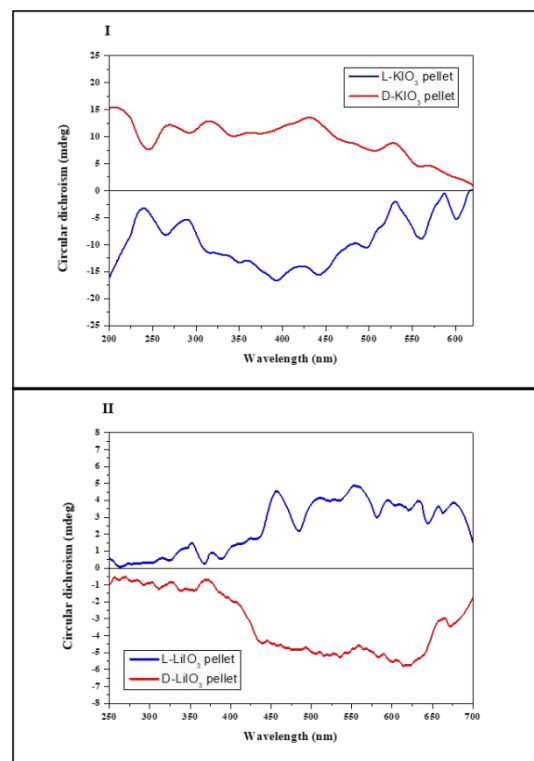

Figure 4 – CD spectra of L/D-Arg-induced KIO$_3$ (I) and L/D-Ala-induced LiIO$_3$ (II) pellets.

The chirality was also measured by low frequency Raman spectroscopy (LFR)[60], a new technique that allows direct measurement of the chirality employing the low-frequency region of the spectrum, which highlights lattice-level interactions and global molecular fluctuations. These lower frequencies are associated with vibrations from weaker bonds and long-range interactions making them highly sensitive to changes in polarization. The enantiomers are excited by fixed polarized light and collected using a movable optical polarization. The polarized light can be horizontal (S-Pol) or vertical (P-Sol). One enantiomer gives a stronger signal for S-Pol, while the other gives a stronger signal for P-Pol.

Aviv *et al.* presented a method that differentiates racemic and enantiopure crystals of amino acids. Intensity changes and wavenumber shifts were seen in single crystals of arginine, aspartic acid and valine[61]. Nematsov *et al.* used LFR to analyze the chiral purity of crystals and showed specific vibrational mode changes as a function of the enantiomeric purity[62]. Moreover, they investigated the dependence of the signal intensity on the orientation of L-Ala single crystals showing correlation between signal intensities with the proximity between the incident beam direction and the orientations of the intermolecular interactions[63]. This makes LFR a powerful method to prove chiral preference by direct measurement.

As iodate salts, the Raman spectroscopy of KIO_3 and $LiIO_3$ are quite similar (Figure S3) and can be divided to three areas: 700-800 cm^{-1} (iodate vibrational modes), 300-400 cm^{-1} (free translational motion of the iodate anion) and 100-200 cm^{-1} (lattice vibrational modes).

We used LFR method to examine the effect of KIO_3 and $LiIO_3$ chiral-induced crystals on the collection of light through a polarizer at different angles (S-Pol and P-Pol), where the enantiomers of the crystal under test are supposed to give opposite effects to each other in intensities at same angles. Moreover, in order to prove the effect precisely, the comparison is of the angles for each crystal separately when the light is collected from the same point in the sample in order to neutralize as many factors as possible that could affect the measurements.

Figure 5I presents the LFR of chiral induced crystals. Higher intensity is evident for the L-chiral inducing KIO_3 crystals when the light is collected at P-Pol with maximum intensity ratio P-Pol/S-Pol of 1.225 at 303 cm^{-1}. In contrast, D-Ala-induced $LiIO_3$ crystals produce higher intensity when the light is collected at S-Pol with maximum S-Pol/P-Pol intensity ratio at 329 cm^{-1} of 1.247 (Figure 5II).

The LFR results support previous measurements. Iodate crystals with higher P-Pol intensity are more prone to be L type, while those with higher S-Pol intensity tend to be D type crystals. Similar results were obtained for D-Arg-induced KIO_3 and L-Ala-induced $LiIO_3$ (Figure S4). LFR signifies long-range interactions where orientation-dependent polarizable interactions prevail. Such interactions are highly responsive to the symmetry of the excitation cone induced by the polarizer and thus provide insight into the crystal chirality.

After proving the chiral preference of our crystals, we used chiral adsorption methods to check their stereoselectivity and chiral discrimination.
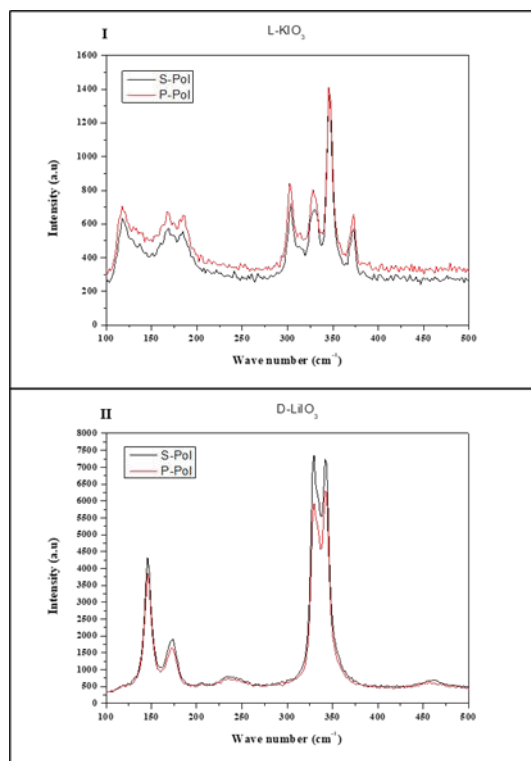

Figure 5 - LFR spectra of L-Arg-induced KIO_3 (I) and D-Ala-induced $LiIO_3$ (II). Black/red curves show signals excited using S/P-Pol.

Chiral selectivity measurements

The adsorption of chiral molecules onto chiral surfaces is a standard way of measuring chirality in solids. Here, we measured the chiral induction on L-Arg-induced KIO_3 and L/D-Ala-induced $LiIO_3$ using CD and polarimeter. In the CD adsorption experiment, a 2.5 mM solution of pure L/D-TA was adsorbed at RT onto different powder concentrations. Figure 6I presents the CD adsorption at 32 mg/mL. The control group which contains the KIO_3 without chiral inducer showed adsorption of ~5% for both L and D-TA without any selectivity at all (green and cyan curves, respectively). However, the addition of the L-Arg to the KIO_3 crystals led to adsorption of 7% for L-TA (red curve) compared to pure L-TA (black curve) and better adsorption of (18%) onto D-TA (pink curve) compared to pure D-TA (blue curve). Figure 6II shows the selectivity of both enantiomers to L-Arg-induced KIO_3; we see better selectivity at all concentrations to D-TA (up to 11%). Moreover, the difference between the enantiomers

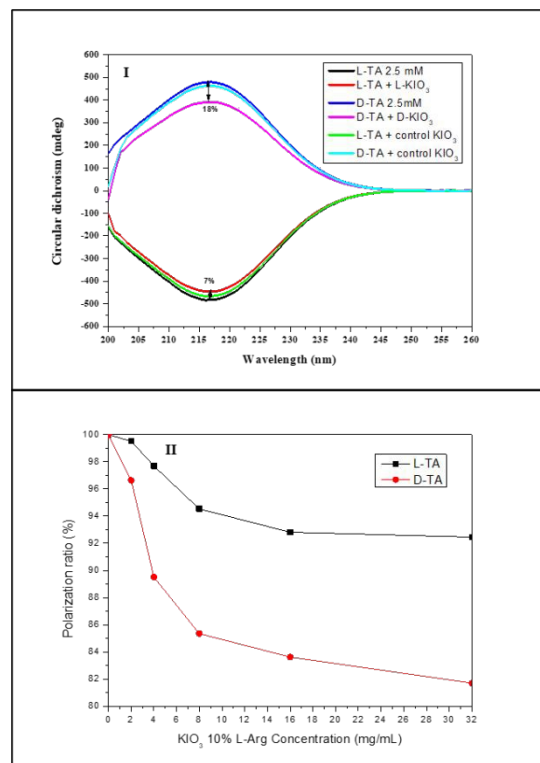increases with increasing concentrations of L-Arg-induced KIO$_3$ crystals.

Figure 6 – Selective chiral adsorption of TA on chiral L-Arg-induced KIO$_3$ crystals: CD spectra of L/D-TA adsorbed onto L-Arg-induced KIO$_3$ (I) and selectivity of L/D-TA at different concentrations (II).

Figure 7I illustrates the CD adsorption at a concentration of 32 mg/mL. Like KIO$_3$, the control group of un-inducing LiIO$_3$ doesn't displayed discernible selectivity with an adsorption of about 20% for both L and D-TA (orange and purple curves, respectively). L-Ala-induced LiIO$_3$ demonstrates enhanced adsorption for L-TA (48%, red curve) compared to pure L-TA (black), while D-TA exhibits 38% absorption (cyan). Superior selectivity is seen at all concentrations, which increases with the crystal concentration up to 10% (Figure 7III). D-Ala-induced LiIO$_3$ on the other hand shows better adsorption for D-TA (34%, green curve) compared to pure D-TA (pink), while L-TA exhibits 23% absorption onto D-Ala-induced LiIO$_3$ (blue). D-Ala-induced LiIO$_3$ crystals show better selectivity for D-TA at all concentrations, with quite similar values up to 11% (Figure 7II).
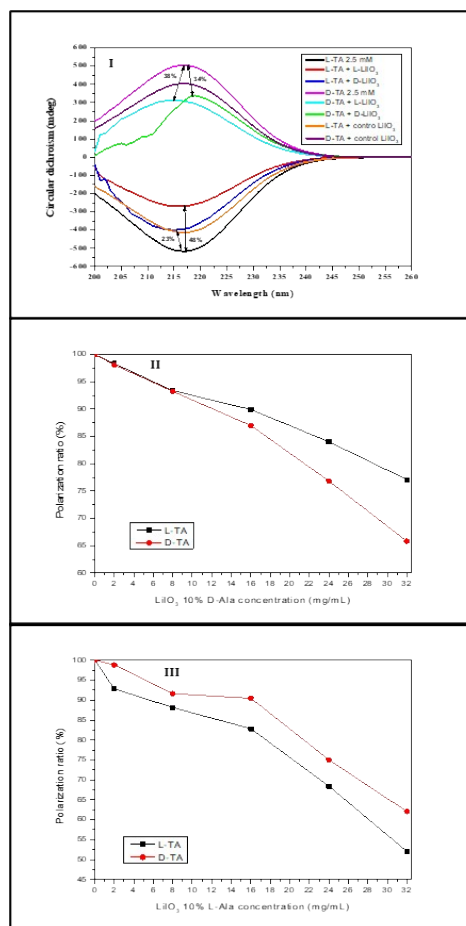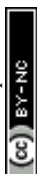

Figure 7 – Selective chiral adsorption of TA on chiral induced LiIO$_3$ crystals – CD spectra of L/D-TA adsorbed onto L/D-Ala-induced LiIO$_3$ (I) and selectivity at different D/L-Ala-induced LiIO$_3$ concentrations (II/III).

To verify that the results obtained indeed show selectivity of the crystals, two additional measurements were made: measuring the mass change of TA enantiomer that did not adsorbed onto the crystals after evaporation of the solvent, and measuring the circular dichroism of racemic solution of TA in order to identify any chiral sign which point to selectivity of the crystals.

Table 1 shows the results for the mass changes of the TA enantiomer that did not adsorbed onto the D-Ala-induced LiIO$_3$ crystals after filtration of the crystals and evaporation of the solvent. We can see that the D-TA mass decreased more (25%) than the L-TA mass (15%) which means the D-Ala-induced LiIO$_3$ crystals are selective in favor to D-TA. Moreover, we notice that the selective percentages are similar to the selectivity we received from the CD (11% and 10% respectively).

Crystal	D-Ala-LiIO$_3$	
Tested enantiomer	L-TA	D-TA
Vial mass (mg)	17683.5	17753.1
Total mass (mg)	17693.7	17762.1
Unadsorbed TA mass (mg)	10.2	9
Decrease from total mass (%)	15	25
Selectivity (%)	10 in favor of D-TA	

Table 1 - Selective chiral adsorption of TA onto D-Ala-induced LiIO$_3$ crystals by measuring the TA mass changes after crystals filtration and solvent evaporation.

Figure 8 presents the circular dichroism measurement of the racemic solution of TA that did not adsorbed onto the D-Ala-induced LiIO$_3$ crystals. The measurement shows negative signals of the solution that indicate of higher presence for the L-TA enantiomer which means the D-Ala-induced LiIO$_3$ crystals are chiral selective in favor to D-TA.
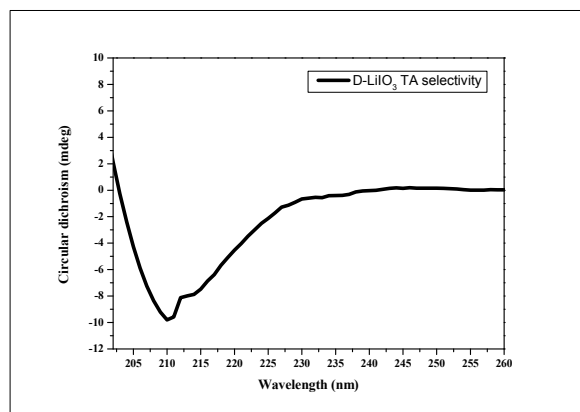

Figure 8 – Selective chiral adsorption of DL-TA on D-Ala-induced LiIO$_3$ crystals.

We also examined the selective chiral adsorption on the crystal surfaces by polarimeter. The polarimeter adsorption experiment included pure L/D-TA 5wt% solution that adsorbed onto L-Arg-induced KIO$_3$ crystals powder concentrations (2, 4, and 8 mg/mL) at RT. Figure 9 presents the selectivity of both TA enantiomers to the L-Arg-induced KIO$_3$ crystals, and like the CD measurements, we can see better selectivity for the D-TA enantiomer for all concentrations. The L-Arg-induced KIO$_3$ shows maximum adsorption of 7% for L-TA at the most concentrated KIO$_3$ compared to the D-TA at the same crystal concentration with maximum adsorption of 24%, therefore, the maximum selectivity we got was 17%. Moreover, we saw by polarimeter the selectivity improvement proves as function of L-Arg-induced KIO$_3$ crystals concentration increase. From the results obtained it can be noted that there is a difference of 6% between the maximum selectivity of L-Arg-induced KIO$_3$ we got from the CD measurements and from the polarimeter. The difference can be explained by the lower sensitivity of the polarimeter which required more concentrated solutions for

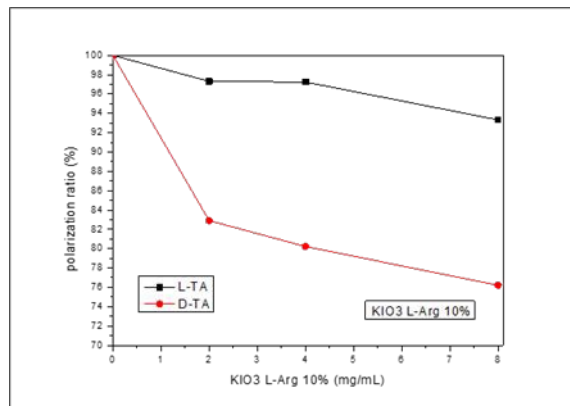measurements that affect the amount of the TA adsorbed onto the L-Arg-induced KIO$_3$.

Figure 9 - Chiral selective adsorption of TA on L-Arg-induced KIO$_3$ crystals by polarimeter.

Chiral separation by crystallization[64-67] is a well-established method whereby a chiral substance such as a chiral resolving agent or solvent is introduced in the crystallization of a racemic mixture. This method typically involves the chiral agent interacting differently with the crystals of each enantiomer during crystallization. In our case, the chiral separation is likely due to the interaction of amino acids with ionic crystal surfaces in a chiral-specific manner. This interaction can influence the nucleation and growth processes by preferentially stabilizing one enantiomer over another. A kinetic study assessed the impact of amino acids on crystallization and chiral separation. Figure 9 shows results for samples collected at various stages of crystallization.

The normal crystallization of KIO$_3$ shows after 4 h crystals with uniform rhombus shape and relatively uniform size of 4.5 μm (Figure 10I). After 12 h crystals of various sizes were obtained resembling a dodecahedron structure with 25 μm size (Figure 10IV). The chiral induced crystallization presents a different phenomenon: L-Arg-induced KIO$_3$ shows an arrangement of square crystals on top of each other that resembles terraces (Figure 10II, V), while D-Arg-induced KIO$_3$ shows such arrangement after 12 h (Figure 10VI) and a trapezoid structure with average size of 4 μm after 4 h (Figure 10III).

It should be noted that we investigated the effect of amino acid concentration on both the crystallization process and chiral induction in the crystals. A series of crystallization experiments were conducted at varying amino acid concentrations, ranging from 1% to 10% by weight relative to the crystal-forming ions. It was found that at concentrations below 10%, no chiral induction was observed. However, starting at 10% (w/w) and above, chiral induction effects were detected and maintained. At higher amino acid

concentrations, no further enhancement in chiral induction was observed.

Our results suggest that amino acids can promote the formation of mesocrystals[68,69] by facilitating the organization of nanocrystals into ordered aggregates. Mesocrystals are crystalline materials consisting of nanometer-sized building blocks often referred to as "nanocrystals" arranged in a regular, repeating pattern. Unlike traditional crystals, composed of a continuous lattice of atoms or molecules, mesocrystals are made up of these smaller, ordered nanocrystals that can be connected in various ways. Overall, it appears that during nucleation amino acids preferentially bind to one chiral face of the crystal, influencing the nucleation rate, resulting in the observed chiral separation.
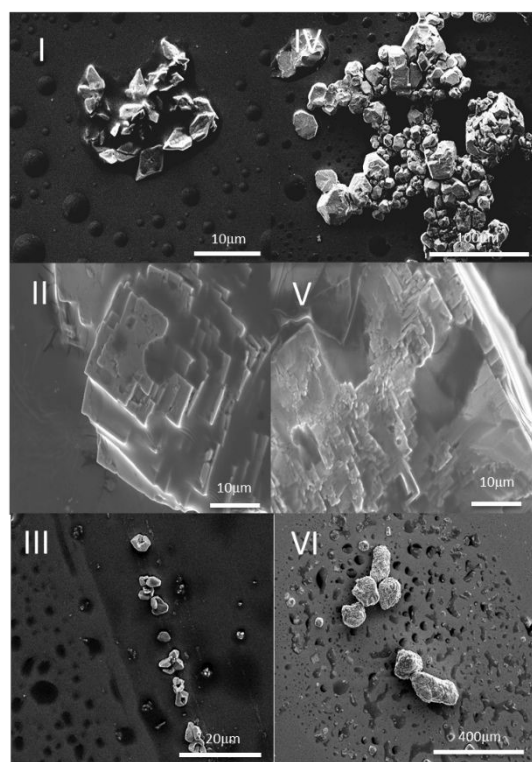

Figure 10 - HR-SEM images of kinetic crystallization of KIO_3 – control KIO_3 crystals after 4/12 h (I/IV, 10/100 μm), L-Arg-induced KIO_3 after 4/12 h (II/V, 10/10 μm) and D-Arg-induced KIO_3 after 4/12 h (III/VI, 20/400 μm).

Conclusions

Chiral induction of the naturally occurring chiral iodate salt minerals KIO_3 and $LiIO_3$ was achieved using chiral alanine and arginine. The resultant crystals varied in morphology, size and surface roughness in contrast to the uniform crystallization obtained without chiral induction. The most prominent change was in the KIO_3 crystals, which transformed from square to hexagonal/deformed shape in D/L-Arg-induced KIO_3. Both chiral-induced $LiIO_3$ crystals exhibited smoother surfaces. L-Ala-induced $LiIO_3$ retained a hexagonal shape, whereas D-Ala-induced $LiIO_3$ displayed an uneven morphology.

The effect of the chiral induction on KIO_3 kinetics was investigated by crystallization at different times. The presence of the chiral inducing molecules was found to affect the arrangement of the KIO_3 crystals by creating mesocrystals with terrace arrangement.

The chiral preference of our crystals was confirmed by various direct measurements including CD of crystal pellets and LFR powder spectroscopy. Significantly, both methods were found to be applicable for direct measurement of the crystal chirality.

The enantioselectivity was also assessed by chiral adsorption measurements on the crystal surface using CD spectroscopy and polarimetry. While L-Arg-induced KIO_3 crystals showed higher selectivity for D-TA, L-Ala-induced $LiIO_3$ showed higher selectivity for L-TA. These findings indicate that L/D-induced crystals do not necessarily improve selectivity for L/D-enantiomers; better improvement may be obtained for the other enantiomers. It should be noted that while our study primarily focuses on chiral induction, we recognize that the reversibility of this process is a crucial factor in understanding the underlying mechanisms. Many chiral crystallization studies have shown that chiral induction by chiral molecules can, in some cases, be reversible under specific conditions, such as changes in pH, temperature, or solvent environment. However, in our experiments, once chirality was induced in the crystallized products, no spontaneous reversal was observed under the experimental conditions used.

Overall, this study provides insight on the chirality of iodate salt crystals within their chiral space group. Study of the chirality and chiral discrimination of naturally occurring chiral minerals such as KIO_3 and $LiIO_3$ is important for understanding the origin of biochemical homochirality and life. Integration of chiral amino acids in the crystallization of naturally occurring chiral minerals is anticipated to provide deeper insight and a more nuanced understanding of the intricate interactions between chiral molecules and crystal surfaces. This approach holds promise for elucidating mechanisms underlying chiral discrimination in inorganic crystals as a holistic process. Utilizing chiral recognition on inorganic surfaces offers advantages across various applications, from asymmetric autocatalysis to chiral sensing and optical functionalities.

Nanoscale Advances Accepted Manuscript

AUTHOR INFORMATION

Department of Chemistry and Institute for Nanotechnology and Advanced Materials, Bar-Ilan University, Ramat Gan 5290002.

Corresponding Author

Prof. Yitzhak Mastai - Yitzhak.Mastai@biu.ac.il

Authors

Matan Oliel - matanoliel5@gmail.com

Notes
The authors declare no competing financial interest.

Conflicts of interest

There are no conflicts to declare.

ASSOCIATED CONTENT

Supporting information is available free of charge via the Internet at: http://pubs.acs.org.
Materials, and FTIR spectra of L/D-Arg-induced KIO_3 and L/D-Ala-induced $LiIO_3$ crystal (**PDF**).

ACKNOWLEDGMENT

Notes and references

1   D. Aquilano, F. Otálora, L. Pastero, and J.M. García-Ruiz, *Progress in Crystal Growth and Characterization of Materials,* 2016, **62 (2)**, 227-251.
2   W. Xu, M. Cheng, S. Zhang, Q. Wu, Z. Liu, M.K. Dhinakaran, F. Liang, E.G. Kovaleva, and H. Li, *Chemical Communications,* 2021, **57 (61)**, 7480-7492.
3   N. Nandi, and D. Vollhardt, *Current Opinion in Colloid & Interface Science* 2008, **13 (1-2)**, 40-46.
4   D.S. Sholl, A. Asthagiri, and T.D. Power, *The Journal of Physical Chemistry B*, 2001, **105 (21)**, 4771-4782.
5   J.I. Putman and D.W Armstrong, *Chirality*, 2022, **34 (10)**, 1338-1354.
6   J.D. Horvath and A.J. Gellman, *Journal of the American Chemical Society*, 2002, **124 (10)**, 2384-2392.
7   C.E. Song, and S.G. Lee, *Chemical Reviews*, 2002, **102 (10)**, 3495-3524.
8   A. Matsumoto, Y. Kaimori, M. Uchida, H. Omori, T. Kawasaki, and K. Soai, *Angewandte Chemie International Edition*, 2017, **56 (2)**, 545-548.
9   T. Cao, Y. Li, L. Tian, H. Liang and K. Qin, *ACS Appl. Nano Mater*, 2018, **1 (2)**, 759-767.
10 D.B. Amabilino, *Chemical Society Reviews*, 2009, **38**, 669-670.
11 D.S. Bag, T.C. Shami and K.U.B. Rao, *Science Journal*, 2008, **58**, 626-635.
12 J. Zhang, M.T. Albelda, Y. Liu and J.W. Canary, *Chirality*, 2005, **17**, 404-418.
13 B.L. Feringa, N.P.M. Huck and A.M. Schoevaars, *Advanced Materials*, 1996, **8**, 681-&.
14 B.L. Feringa, R.A. van Delden, N. Koumura and E.M. Geertsema, *Chemical Reviews*, 2000, **100**, 1789-1816.
15 B.L. Feringa, *Accounts of Chemical Research*, 2001, **34**, 504-513.
16 X.Y. Zhao, S.S. Perry, J.D. Horvath and A.J. Gellman, *Surf Sci*, 2004, **563**, 217-224.
17 C.F. McFadden, P.S. Cremer and A.J. Gellman, *Langmuir*, 1996, **12**, 2483-2487.
18 K.H. Ernst, *Current Opinion in Colloid & Interface Science*, 2008, **13**, 54-59.
19 A.J. Gellman, *Acs Nano*, 2010, **4**, 5-10.
20 A. Kuhnle, T.R. Linderoth and F. Besenbacher, *Top Catal*, 2011, **54**, 1384-1391.
21 S.M. Barlow and R. Raval, *Surface Science Reports*, 2003, **50**, 201-341.
22 Y. Mastai, *Chemical Society Reviews*, 2009, **38**, 772-780.
23 L. Thomsen, A. Tadich, D.P. Riley, B.C.C. Cowie and M.J. Gladys, *Journal of Physical Chemistry C*, 2012, **116**, 9472-9480.
24 R. Oda, F. Artzner, M. Laguerre and I. Huc, Journal of the American Chemical Society, 2008, **130**, 14705-14712.
25 A.E. Baber, A.J. Gellman, D.S. Sholl and E.C.H. Sykes, *Journal of Physical Chemistry C*, 2008, **112**, 11086-11089.
26 C. Roth and K.H. Ernst, *Top Catal*, 2011, **54**, 1378-1383.
27 G. Shemer, O. Krichevski, G. Markovich, T. Molotsky, I. Lubitz and A.B. Kotlyar, *Journal of the American Chemical Society*, 2006, **128**, 11006-11007.
28 C. Gautier and T. Burgi, *Journal of the American Chemical Society*, 2006, **128**, 11079-11087.
29 C. Gautier and T. Burgi, *Journal of the American Chemical Society*, 2008, **130**, 7077-7084.
30 O. Álvarez-Bermúdez, K. Landfester, K.A.I. Zhang and R. Muñoz-Espí, *Macromolecular rapid communications*.
31 L.C. Preiss, M. Wagner, Y. Mastai, K. Landfester and R. Muñoz-Espí, *Macromolecular rapid communications*, 2016, **37**, 1421-1426.
32 L.C. Preiss, L. Werber, V. Fischer, S. Hanif, K. Landfester, Y. Mastai and R. Muñoz-Espí, *Adv. Mater*, **27**, 2728-2732.
33 P. Paik, Y. Mastai, I. Kityk, P. Rakus and A. Gedanken, *Journal of solid state chemistry*, 2012, **192**, 127-131.
34 R. Oda, I. Hue, M.C.D.J. Schmutz, S.J. Candau and F.C. MacKintosh, *Nature*, 1999, **399**, 566-569.
35 K. Sugiyasu, S.I. Tamaru, M. Takeuchi, D. Berthier, I. Hue, R. Oda and S. Shinkai, *Chemical communications*, 2002, **11**, 1212-1213.
36 F. Freire, J.M. Seco, E. Quiñoá and R. Riguera, *Angewandte Chemie International Edition*, 2011, **50**, 11692-11696.

Nanoscale Advances Accepted Manuscript

37 F. Freire, J.M. Seco, E. Quiñoá and R. Riguera, *Journal of the American Chemical Society*, 2012, 134, 19374-19383.

38 M. Lui, L. Zhang and T. Wang, *Chemical reviews*, 2015, **115**, 7304-7397.

39 L. Zhang, T. Wang, Z. Shen and M. Liu, *Advanced Materials*, 2016, **28**, 1044-1059.

40 T. Cao, L. Mao, Y. Qiu, L. Lu, A. Banas, K. Banas, R.E. Simpson and H.C. Chui, *ADVANCED OPTICAL MATERIALS*, 2019, **7 (3),** 1801172.

41 J. Morales-Vidal, N.R. López, and M.A. Ortuño, *The Journal of Physical Chemistry C*, 2019, **123 (22)**, 13758-13764.

42 Ž. Šljivančanin, K.V. Gothelf, and B. Hammer, *Journal of the American Chemical Society*, 2002, **124 (49)**, 14789-14794.

43 A. Ben-Moshe, S.G. Wolf, M.B. Sadan, L. Houben, Z. Fan, A.O. Govorov, and G. Markovich, *Nature Communications*, 2014, **5 (1)**, 1-9.

44 R.M. Hazen, and D.A. Sverjensky, *Cold Spring Harbor Perspectives in Biology*, 2010, **2 (5)**, a002162.

45 W. Jiang, M.S. Pacella, D. Athanasiadou, V. Nelea, H. Vali, R.M. Hazen, J.J. Gray, and M.D. McKee, *Nature Communications*, 2017, **8 (1)**, 1-13.

46 R.M. Hazen, and D.S. Sholl, *Nature Materials*, 2003, **2 (6)**, 367-374.

47 Y. Tanaka, T. Takeuchi, S.W. Lovesey, K.S. Knight, A. Chainani, Y. Takata, M. Oura, Y. Senba, H. Ohashi, and S. Shin, *Physical Review Letters*, 2008, **100 (14)**, 145502.

48 G. Otis, M. Nassir, M. Zutta, A. Saady, S. Ruthstein, and Y. Mastai, *Angewandte Chemie*, 2020, **132 (47)**, 21110-21115.

49 P. Cintas, P, *Angewandte Chemie International Edition*, 2002, **41 (7)**, 1139-1145.

50 A. Ben-Moshe, S.G. Wolf, M.B. Sadan, L. Houben, Z. Fan, A.O. Govorov, and G. Markovich, *Nature Communications*, 2014, **5 (1)**, 1-9.

51 R.M. Hazen, T.R. Filley, and G.A. Goodfriend, *Proceedings of the National Academy of Sciences*, 2001, **98 (10)**, 5487-5490.

52 J. Jumas, A. Goiffon, B. Capelle, A. Zarka, J. Doukhan, J. Schwartzel, J. Detaint, and E. Philippot, *Journal of crystal growth*, 1987, **80 (1)**, 133-148.

53 Y. Muraoka, and K. Kihara, *Physics and Chemistry of Minerals*, 1997, **24 (4)**, 243-253.

54 P. Prado-Herrero, J. Garcia-Guinea, E. Crespo-Feo, and V. Correcher, *Phase Transitions*, 2010, **83 (6)**, 440-449.

55 L. Bayarjargal, L. Wiehl, and A. Friedrich et al, *J Phys Condens Matter*, 2012, **24 (32)**.

56 H. Kasatani, S. Aoyagi, Y. Kuroiwa, K. Yagi, R. Katayama, and H. Terauchi, *Nucl Instruments Methods Phys Res Sect B Beam Interact with Mater Atoms*, 2003, **199**, 49-53.

57 L. Liu, R.Q. Wu, Z.H. Ni, Z.X. Shen, and Y.P. Feng, *J Phys Conf Ser*, 2006, **28(1)**, 105-109.

58 R. Ashok Kumar, R. Ezhil Vizhi, N. Vijayan, and D. Rajan Babu, *Sch Res Libr*, 2011, **2(4)**, 373-383.

59 A. Silambarasan, P. Rajesh, and P. Ramasamy et al, *Bull Mater Sci*, 2017, **40(4)**, 783-789.

60 V. Damle, H. Aviv, and Y.R. Tischler, *Anal. Chem*, 2022, **94**, 3188-3193.

61 H. Aviv, I. Nematsov, Y. Mastai, and Y.R. Tischler, *J. Phys. Chem. A*, 2017, **121(41)**, 7882-7888.

62 I. Nematsov, Y. Mastai, Y.R. Tischler, and H. Aviv, *Chem. Phys. Chem*, 2018, **19(22)**, 3116-3121.

63 I. Nematsov, H. Aviv, Y. Mastai, and Y.R. Tischler, *Crystals*, 2019, **9(8)**, 425.

64 I Weissbuch, L. Addadi, M. Lahav, and L. Leiserowitz, *Science*, 1991, **253(5020)**, 637-645.

65 G. Coquerel, *Novel Optical Resolution Technologies*, 2007, **269**, 1-51.

66 H. Lorenz, and A. Seidel-Morgenstern, *Angewandte Chemie*, 2014, **53(5)**, 1218-1250.

67 H. Cölfen, and M. Antonietti, *Angewandte Chemie*, 2005, **44(35)**, 5576-5591.

68 M. Niederberger, and H. Coelfen, *Physical Chemistry Chemical Physics*, 2006, **8(28)**, 3271-3287.

69 X. Xia, J. Tu, Y. Zhang, X. Wang, C. Gu, X. Zhao, H.J. Fan, *Acs Nano*, 2012, **6(6)**, 5531-5538.

ARTICLE

Nanoscale Advances Accepted Manuscript

Prof. Yitzhak Mastai
Department of Chemistry and the Institute of Nanotechnology Bar-Ilan University, Israel.

פרופ' יצחק מסתאי
המחלקה לכימיה אוניברסיטת בר אילן
רמת גן ישראל

View Article Online
DOI: NA01006J

Thursday, 21 November 2024

To

Prof. Dirk Guldi

Associate Editor, Nanoscale

Manuscript ID: NR-ART-09-2024-003843

Data Availability Statement

The data that support the findings of this study are available from the corresponding author upon reasonable request. Experimental data, including raw spectra and additional supplementary information, are included in the manuscript and its supporting files. Data not included in the manuscript are available upon request, and all relevant materials will be made accessible to qualified researchers for non-commercial purposes.

Sincerely,

Prof. Dr. Yitzhak Mastai

Tel: 03-531-7681 טל • Fax: 03-738-4053 :פקס   E-mail: Mastai@biu.ac.il

Bar-Ilan University Ramat Gan 5290002, Israel 5290002 אוניברסיטת בר אילן רמת גן

www.biu.ac.il